RSC Advances

PAPER

View Article Online
View Journal | View Issue

Cite this: *RSC Adv.*, 2026, **16**, 13420

Utilizing high-energy photons *via* energy transfer for the performance enhancement of PTB7-Th:COi8DFIC-based organic solar cells

Anoop C Sathyadevan Nair, [a] K. P. Adarsh Raj,[a] Muneendra Dasannagari,[b] Abhijith T, [cd] Abhishek Melarkode Rajendran,[a] Dipangkor Basumatary, [a] Safakath Karuthedath, [*b] C. S. Suchand Sangeeth [*a] and Vari Sivaji Reddy [*a]

Fine-tuning the photophysical properties and nanoscale morphology of the photoactive layer by incorporating an additional donor or acceptor is a promising strategy for improving the performance of organic solar cells (OSCs). Here, we strategically incorporated a wide-bandgap donor (PBDB-T) into the PTB7-Th:COi8DFIC-based host binary to attain a relatively high power conversion efficiency (PCE). The complementary absorption spectra of these materials enabled the harvesting of solar spectrum in a wide wavelength range of 400 nm to 1000 nm. An efficient energy transfer from PBDB-T to PTB7-Th was confirmed by steady-state and time-resolved photoluminescence measurements. The introduction of PBDB-T resulted in an optimized active layer morphology, thereby markedly improving the exciton-dissociation and charge-collection efficiencies, leading to the improvement of the short-circuit current density (J_{SC}) and fill factor (FF). As a result, ternary OSCs fabricated with 20 wt% PBDB-T exhibited an average efficiency of 9.74%, compared to 8.87% in the host binary. Impedance spectroscopy analysis at various bias voltages within the operating regime revealed a reduction in the bulk resistance and an increase in the recombination resistance for the optimized ternary OSC, validating the observed enhancements in J_{SC} and FF. Furthermore, transient photovoltage and photocurrent measurements revealed a long carrier lifetime of 22.30 μs and a short extraction time of 904 ns in the ternary system, which were beneficial for the OSC performance. In addition, the incorporation of PBDB-T resulted in reduced non-radiative recombination in the device through efficient energy transfer. The role of PBDB-T in improving the performance of the PTB7-Th:COi8DFIC-based host binary was investigated through systematic photophysical, morphological and electrical characterizations.

Received 16th November 2025
Accepted 26th February 2026

DOI: 10.1039/d5ra08837b

rsc.li/rsc-advances

1. Introduction

Organic solar cells (OSCs) are considered as one of the top choices to fulfill the future energy requirements due to their versatile properties, such as low cost, flexibility, large area printing, light weight and solution processability.[1–5] Effective photon harvesting in a wide wavelength range is of high interest in the field of photovoltaics. In binary OSCs consisting of a donor (D) and an acceptor (A), the narrow absorption window of organic semiconductors limits the harvesting of a broad solar spectrum, even though they possess high absorption coefficients.[6,7] While the low-energy photons in the near infrared (NIR) region are available for exciton generation due to the development of various non-fullerene acceptors, harvesting the entire visible and NIR spectrum using a binary architecture remains a challenge.[8–10] In order to overcome this problem, tandem device architecture, which consists of different single junction sub cells having complimentary bandgaps stacked one over the other, was introduced.[11–13] The front sub cell harvests the high-energy photons, whereas the back sub cell, which contains narrow-bandgap materials, utilizes the low-energy photons for exciton generation. Even though the tandem structure is efficient in photon harvesting, the increased fabrication complexity and high production cost make it less suitable for practical applications.[14,15]

Ternary OSC architecture, which uses a blend of three materials (D1:D2:A or D:A1:A2), with complementary absorption spectra as the active layer, has been introduced as an alternative to the tandem architecture for harvesting photons in a broad wavelength range.[16–19] Along with broad range absorption, the ternary OSCs are often benefitted by additional charge

[a]*Department of Physics, National Institute of Technology Calicut (NITC), Kerala – 673601, India. E-mail: sivaji@nitc.ac.in*

[b]*Institute of Materials Research, Tsinghua Shenzhen International Graduate School, Tsinghua University, Shenzhen – 518055, China*

[c]*Department of Physics, PSG Institute of Technology and Applied Research, Neelambur, Coimbatore, Tamil Nadu – 641062, India*

[d]*Department of Nanoscience and Technology, PSG Institute of Advanced Studies, Peelamedu, Coimbatore, Tamil Nadu – 641004, India*

transfer, energy transfer, parallel linkage and alloy mechanisms.[20–23] Recently, a power conversion efficiency (PCE) above 20% has been achieved using the ternary strategy.[24–27] Selecting a suitable third component is of great importance in ternary OSCs, as it can significantly affect the nanoscale morphology of the blend, which in turn directly influences the performance of OSCs.

In the present study, we have selected a less explored PTB7-Th:COi8DFIC blend as the host binary. COi8DFIC is an A-D-A type molecule with eight fused rings in the D domain and two difluoro-substituted end groups in the A domains, often blended with PTB7-Th in OSCs due to proper energy level alignment, favorable phase separation and optimal nano-scale morphology.[28–32] Moreover, COi8DFIC exhibits one of the longest reported exciton diffusion lengths (≈40 nm) to date, which is suitable for efficient exciton dissociation.[33] These properties make COi8DFIC a promising candidate for high-performance OSC applications. Various strategies have been employed to improve the performance of PTB7-Th:COi8DFIC-based OSCs. Zhang *et al.* used 0.5 vol% of 1,8-diiodooctane as the solvent additive, which interacted with the side chains of COi8DFIC to enhance the formation of A-D-type J aggregates in the blend.[31] The significant red shift of the absorption spectrum towards the near-infrared region has resulted in a substantial improvement in the PCE. Li *et al.* achieved a PCE of 13.4% by employing the hot substrate casting method to simultaneously form H and J aggregates of COi8DFIC, which spread the absorption spectrum towards both low and high wavelengths.[30] Ternary bulk-heterojunction strategy has also been explored to improve the performance of PTB7-Th:COi8DFIC-based OSCs by adding IEICO-4F, ITIC-4F and $PC_{70}BM$ as the third component into the host binary.[34–37] Both IEICO-4F and ITIC-4F absorb in the high wavelength region. Even though $PC_{70}BM$ absorbs in the low wavelength region, its contribution to the light harvesting in OSCs is limited due to relatively modest optical absorption.[38] Therefore, the addition of a wide bandgap material with strong absorption into PTB7-Th:COi8DFIC seems to be a promising method for harvesting high-energy photons.

Here, we select a wide bandgap polymer (PBDB-T) as the third component. The good compatibility between PBDB-T and the host donor (PTB7-Th), together with the complementary absorption ranges of the ternary components, is expected to provide favorable morphological properties and enhanced spectral coverage. Inverted OSCs are fabricated with PBDB-T:PTB7-Th:COi8DFIC as the active layer, and the weight percent of PBDB-T in the blend is optimized to achieve the best performance. The optimum ternary OSC with 20 wt% PBDB-T exhibited an average efficiency of 9.74%, compared to 8.87% for the PTB7-Th:COi8DFIC host binary. The transient photocurrent (TPC) measurement on the optimized devices reveals that the carrier extraction time for the ternary device is reduced to 904 ns, compared to 1019 ns for the host binary device. Correspondingly, the carrier lifetime (obtained from the transient photovoltage (TPV) experiments) in the ternary device is improved to approximately 22.30 μs, which is more than three times that of the host binary (≈6.35 μs). Based on various photophysical, morphological and electrical characterizations, the performance enhancement mechanism has been thoroughly investigated.

2. Experimental

Inverted organic solar cells were fabricated with the following device structure: indium tin oxide (ITO)/ZnO/photoactive layer/MoO_3/Ag. ZnO precursor solution was prepared according to the method described in the literature and spun on top of oxygen-plasma-treated ITO substrates at a speed of 4000 rpm for 40 s.[39] This was followed by annealing the substrates at 180 °C for 12 min. The active layer solution with a D:A weight ratio of 1:1.5 was prepared at a concentration of 15 mg mL^{-1} by dissolving donor and acceptor molecules in chlorobenzene, with 1,8-diiodooctane (1% V/V) as solvent additive. The solution was stirred overnight at 80 °C. The active layer solution was spun on top of ZnO at 1000 rpm for 60 s. Finally, 7 nm-thick MoO_3 and 100 nm-thick Ag films were thermally evaporated through a shadow mask, making the device area 9 mm^2. All active layer materials, MoO_3, solvents and ZnO precursors were purchased from Sigma-Aldrich and used as received. The current density–voltage (*J–V*) characteristics of OSCs were measured under AM 1.5 G illumination (Photo emission tech solar simulator # SS50AAA) using a precision source/measure unit (Agilent, B2902A). A Newport, Oriel–IQE 200 system was employed to measure the external quantum efficiency (EQE) of the devices. The optical absorption spectra of the active layer materials were measured using a spectrophotometer (PerkinElmer, LAMBDA 365). Steady-state photoluminescence (PL) measurements were carried out using a fluorescence spectrophotometer (Horiba, Fluorolog-3 TCSPC). Fluorescence decay dynamics were recorded using a TCSPC lifetime fluorometer (Horiba, DeltaFlex). The surface morphology of the active layer film was measured using atomic force microscopy (AFM) (NT-MDT, Micro 40). The contact angle measurements on the active material films with water and ethylene glycol were carried out using a Holmarc (HOIADCAM-01A) contact angle meter. The AC impedance measurements at various bias voltages were carried out using an LCR meter (ZM2376, NF Corporation) at frequencies from 10 Hz to 2 MHz under 1 sun illumination. TPC and TPV measurements were conducted using the PAIOS electro-optical characterization module (Fluxim Co., Switzerland), integrated with the Setfos-Paios numerical simulation module.[33] A white light LED (400–780 nm) with a pulse width of 15 μs was used for the measurement.

3. Results and discussion

Fig. 1(a) shows the chemical structures of PBDB-T (D1), PTB7-Th (D2) and COi8DFIC (A) used as active layer materials in the present study. The UV-vis absorption spectra of these materials are presented in Fig. 1(b). The guest donor, PBDB-T, absorbed from 400 nm to 700 nm, whereas the absorption spectrum of the host donor, PTB7-Th, spanned from 500 nm to 800 nm. The absorption of the acceptor, COi8DFIC, was predominantly in the NIR region (600–1000 nm). By incorporating PBDB-T as the third component in the PTB7-Th:COi8DFIC binary blend,

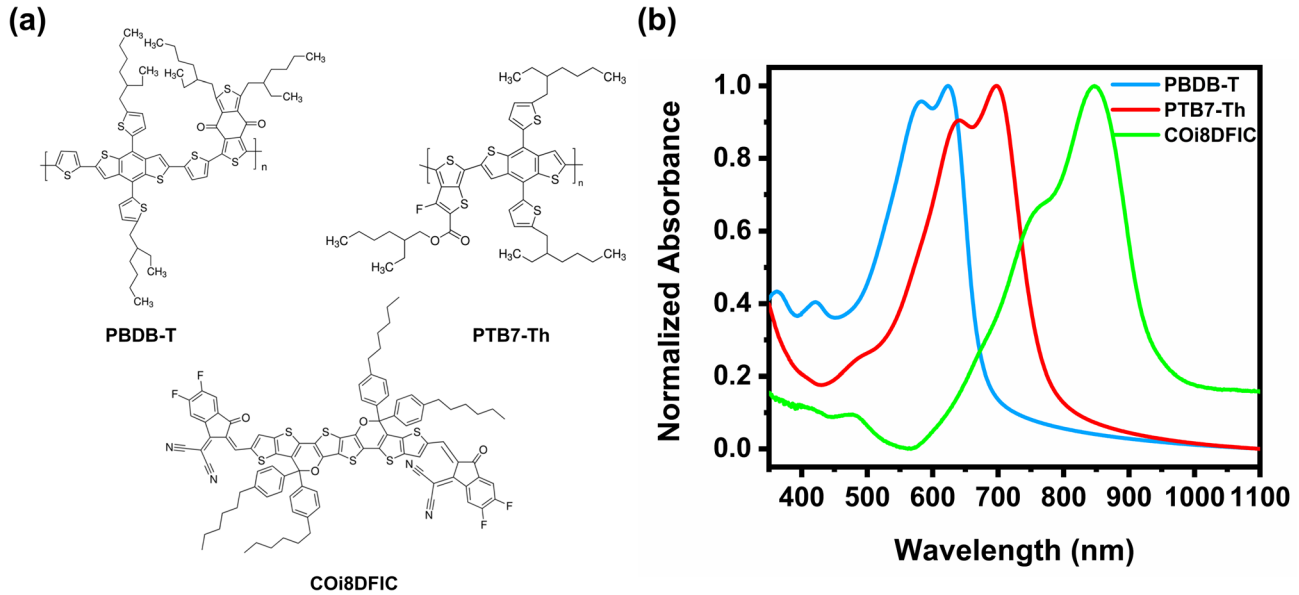

Fig. 1 (a) Chemical structures of PBDB-T, PTB7-Th and COi8DFIC and (b) normalized UV-vis absorption spectra of the PBDB-T, PTB7-Th and COi8DFIC neat films.

photons in a broad wavelength range from 400 nm to 1000 nm could be harvested, which was beneficial for boosting the device performance.

To explore the photovoltaic performance of the proposed ternary combination, OSCs were fabricated with the following device structure: ITO/ZnO/PBDB-T:PTB7-Th:COi8DFIC/MoO_3/Ag, as depicted in Fig. 2(a). The weight ratio of PBDB-T was varied from 0% to 100% in order to optimize the device performance. The UV-vis absorption spectra of ternary blend films with different D1:D2 weight ratios (0:1, 0.2:0.8, 0.8:0.2, and 1:0) are shown in Fig. 2(b). Fig. S1 presents the spectra for all tested D1:D2 weight ratios. As expected, the introduction of PBDB-T improved the absorption at low wavelengths, allowing high-energy photons to contribute more efficiently to exciton generation. Moreover, no change in the absorption peak position of COi8DFIC was observed due to the presence of PBDB-T (Fig. 2(b)), indicating no effect of PBDB-T on COi8DFIC aggregation. Fig. 2(c) represents the *J*–*V* curves of OSCs fabricated with different D1:D2 weight ratios. The corresponding photovoltaic parameters are presented in Table 1. The host binary consisting of PTB7-Th:COi8DFIC exhibited an average PCE of 8.87% with a J_{SC} of 19.86 mA cm^{-2}, a V_{OC} of 0.721 V and an FF of 61.93%. The addition of 20 wt% PBDB-T in the donor resulted in the highest PCE of 9.74% with a J_{SC} of 21.36 mA cm^{-2}, a V_{OC} of 0.726 V and an FF of 62.80%. Further increase in the PBDB-T content resulted in a steady reduction in PCE (Fig. S2 and Table S1). As shown in Table 1, OSCs with 80% PBDB-T showed an average PCE of 8.15%. Following the same trend, PBDB-T-based binary showed a poor PCE of 6.81%, mainly due to a relatively low FF of 52.91%. This could be attributed to the incompatible blend of PBDB-T and COi8DFIC, leading to inadequate charge transport. Moreover, the box plot of the PCE shown in Fig. S3 confirms the reproducibility of the experimental results. In order to study the spectral response of the devices, EQE measurements were carried out, and the spectra are presented in Fig. 2(d). The optimum ternary device with 20 wt% PBDB-T in the donor exhibited superior quantum efficiency, reaching 70% at 850 nm. Additionally, the maximum EQE of all the devices was found to be around 850 nm due to the high amount of COi8DFIC in the blend. It also indicated efficient hole transfer from COi8DFIC to the donors, especially to PTB7-Th, as evident from the FF values. The low EQE values observed for the PBDB-T:COi8DFIC binary device in the absorption range of PBDB-T indicated the poor exciton dissociation and charge transport in the blend compared to those of the ternary devices.

To investigate the possibility of energy transfer from the wide-bandgap PBDB-T to the medium-bandgap PTB7-Th, steady-state PL measurements were performed. As shown in Fig. 3(a), the absorption spectrum of PTB7-Th strongly overlaps with the emission spectrum of PBDB-T, indicating possible energy transfer from PBDB-T to PTB7-Th.[40,41] To understand the energy transfer mechanism in more detail, the PL measurements were carried out on D1:D2 blend films with various weight ratios. The solutions were prepared at a concentration of 10 mg mL^{-1} and spun at 1000 rpm to ensure equal thickness for all the samples. For PL measurements, samples were excited at a wavelength of 620 nm, which was closer to the absorption maximum of PBDB-T (623 nm), and the PL spectra of the films are shown in Fig. 3(b). The emissions of pristine PBDB-T and PTB7-Th films were found to be in the ranges of 625–850 nm and 700–875 nm, respectively. The emission intensity of pristine PTB7-Th was only half of that of pristine PBDB-T, indicating less absorption by PTB7-Th. When a small amount of PTB7-Th was added to PBDB-T, significant quenching in the emission intensity of PBDB-T with a simultaneous increase in the emission intensity of PTB7-Th was observed, confirming

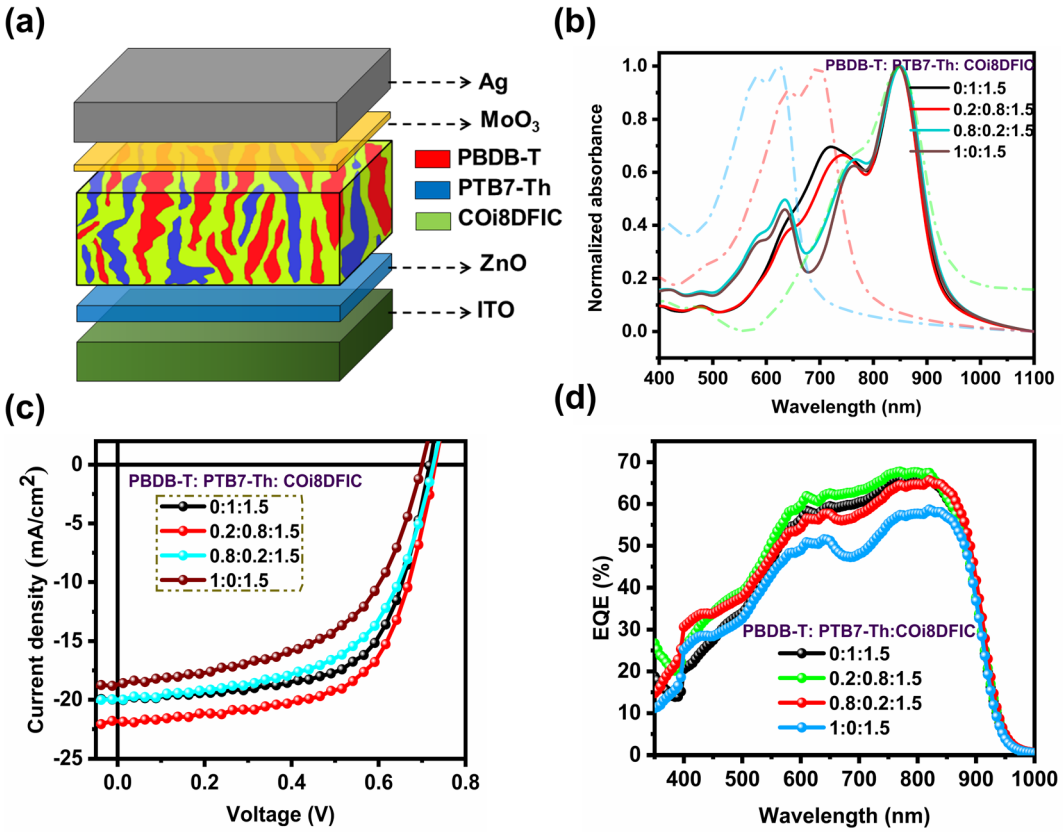

Fig. 2 (a) Device structure of inverted OSCs and (b) UV-vis absorption spectra of active-layer thin films; the dotted lines represent the UV-vis absorption spectra of pristine molecules. (c) Light J–V characteristics and (d) EQE spectra of OSCs fabricated with various PBDB-T:PTB7-Th weight ratios.

Table 1 Photovoltaic parameters of OSCs with different PBDB-T:PTB7-Th weight ratios

				PCE (%)	
PBDB-T:PTB7:COi8DFIC	J_{SC} (mA cm^{-2})	V_{OC} (V)	FF (%)	Average	Best
0:1:1.5	19.86 ± 0.67	0.721 ± 0.003	61.93 ± 1.81	8.87 ± 0.24	9.16
0.2:0.8:1.5	21.36 ± 0.36	0.726 ± 0.004	62.80 ± 0.48	9.74 ± 0.17	9.98
0.8:0.2:1.5	20.05 ± 0.43	0.721 ± 0.006	56.31 ± 1.11	8.15 ± 0.15	8.34
1:0:1.5	18.15 ± 0.37	0.708 ± 0.006	52.91 ± 1.04	6.81 ± 0.13	7.06

energy transfer from PBDB-T to PTB7-Th.[42] Moreover, it was noted that the maximum emission intensity of PTB7-Th in the blend film was observed for the sample containing 20% PTB7-Th and 80% PBDB-T. As the fraction of PTB7-Th increased in the blend, the emission intensity of PTB7-Th was consistently reduced. These results clearly indicated that the major portion of the PTB7-Th emission in the blend was contributed by energy transfer from PBDB-T.

The cascade energy level alignment between the components of the ternary blend hinted at the possibility of exciton dissociation at the PBDB-T/PTB7-Th interface. To get more insight into the charge/energy transfer mechanisms, time-resolved photoluminescence (TRPL) measurements were carried out. Fig. S5 shows the normalized PL spectra of the PBDB-T and PTB7-Th thin films with emission peaks at 725 and 770 nm, respectively. The TRPL spectra of the pristine PBDB-T and PTB7-Th films monitored at 725 and 770 nm, respectively, are presented in Fig. 4(a). The decay curves were fitted using the bi-exponential model, $A + B_1e^{-t/\tau_1} + B_2e^{-t/\tau_2}$, where A is the offset correction term representing the ambient light and instrumental noise.[43] The average lifetime was calculated using the following equation:

$$\tau_{ave} = \frac{B_1\tau_1 + B_2\tau_2}{B_1 + B_2} \quad (1)$$

The PBDB-T exhibited an average lifetime of 288 ps at 725 nm, whereas the lifetime of PTB7-Th was found to be 131 ps at 770 nm. As presented in Fig. 4(b), after adding 20% PBDB-T into the donor, the lifetime of PBDB-T drastically reduced to 88

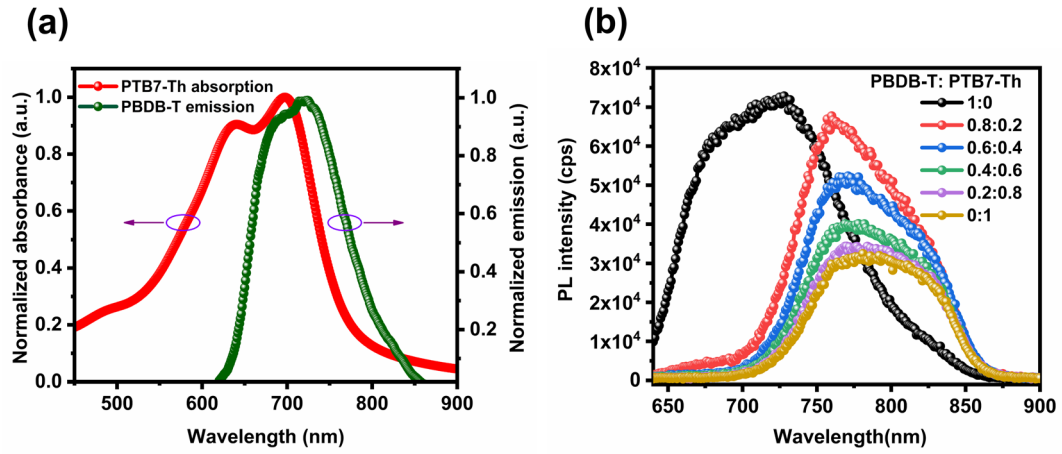

Fig. 3 (a) Normalized UV-vis absorption spectrum of PTB7-Th and the normalized PL spectrum of the PBDB-T film. (b) PL spectra of the PBDB-T:PTB7-Th blend films with various weight ratios.

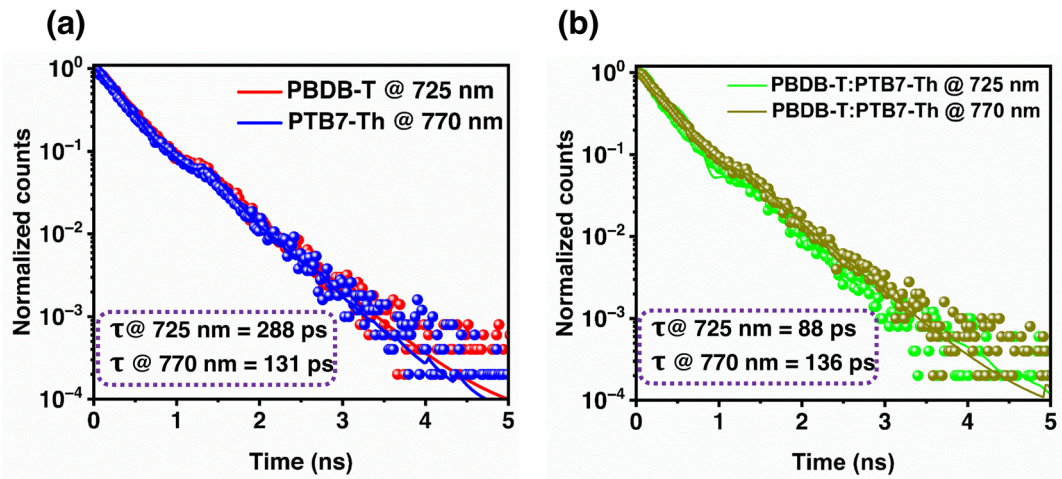

Fig. 4 TRPL spectra of (a) PBDB-T and PTB7-Th, and (b) PBDB-T:PTB7-Th thin films monitored at 725 and 770 nm. All the samples were excited at 630 nm.

ps, while the lifetime of PTB7-Th in the blend increased to 136 ps, indicating an efficient energy transfer from PBDB-T to PTB7-Th.[44–46] The efficiency of energy transfer from PBDB-T to PTB7-Th was calculated using the following equation:

$$\eta = 1 - \frac{\tau_{DA}}{\tau_D} \quad (2)$$

where τ_{DA} and τ_D are the PL lifetimes of energy donor with and without energy acceptor.[47] The energy transfer efficiency was calculated to be 70% for the blend with 20% PBDB-T. To further exclude the possibility of exciton dissociation at the D1/D2 interface, devices were fabricated with PBDB-T, PTB7-Th and PBDB-T:PTB7-Th (0.2:0.8) as the active layers without COi8DFIC. The corresponding *J*–*V* curves are presented in Fig. S6. The PBDB-T- and PTB7-Th-based devices exhibited a J_{SC} of 0.47 mA cm^{-2} and 0.28 mA cm^{-2}, respectively. The J_{SC} value of the PBDB-T:PTB7-Th device (0.38 mA cm^{-2}) was between that of the individual donor-based devices, indicating negligible exciton dissociation at the PBDB-T/PTB7-Th interface.[48]

Both PBDB-T and PTB7-Th consist of a benzodithiophene group in their backbones, hinting at possible alloy formation between the donors. To verify this possibility, contact angle measurements were carried out on pristine PBDB-T and PTB7-Th thin films. Water and ethylene glycol (EG) with known surface energy values and different polarities on the film surface were used to obtain accurate surface energy values.[49,50] The images of droplets are presented in Fig. S7. PBDB-T exhibited a water contact angle of 95.58° ± 0.62°, whereas PTB7-Th exhibited a slightly higher value of 101.59° ± 0.71°. On the other hand, both PBDB-T and PTB7-Th showed relatively low EG contact angles of 80.60° ± 0.39° and 74.76° ± 0.77°, respectively. The surface energy of the materials was calculated using the harmonic mean formula presented in the supplementary information. PBDB-T exhibited a surface energy of 27.76 m Nm^{-1}, with a polar component of 1.38 m Nm^{-1} and a dispersive component of 26.38 m Nm^{-1}. Similarly, the surface energy of PTB7-Th was found to be 24.36 m Nm^{-1}, with a polar

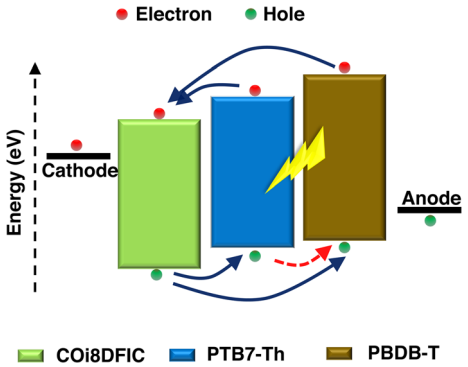

Fig. 5 Schematic showing the energy transfer between the donors and charge transport pathways.

component of 4.53 m Nm^{-1} and a dispersive component of 19.84 m Nm^{-1}. The interfacial energy between the donors was calculated by Wu's method:[51]

$$\gamma_{x:y} = \gamma_x + \gamma_y - 4\frac{\gamma_x^d \gamma_y^d}{\gamma_x^d + \gamma_y^d} - 4\frac{\gamma_x^p \gamma_y^p}{\gamma_x^p + \gamma_y^p} \quad (3)$$

where $\gamma_{x:y}$ is the interfacial energy between material x and y, and γ_x and γ_y are the surface energies of pristine materials, calculated from the contact angle measurements. A large interfacial energy of 2.64 m Nm^{-1} was found between PBDB-T and PTB7-Th, making the formation of organic alloy thermodynamically less probable.[52,53]

From these analyses, we concluded that energy transfer was the main mechanism responsible for performance enhancement. The working of ternary OSC are schematically presented in Fig. 5. The excitons in both PBDB-T and PTB7-Th dissociated at their respective interfaces with COi8DFIC. The electrons were collected at the cathode through the COi8DFIC channel, and the holes preferred to take the individual D1 or D2 channel to the anode. Even though the hole transport from PTB7-Th to PBDB-T was energetically feasible, the small amount of PBDB-T in the blend made it less probable (indicated by the dashed red arrow in the schematic).

To understand the effect of PBDB-T on the morphology of the active layer blend, AFM analysis was carried out, and the results are presented in Fig. 6. Fig. 6 (a–d) shows the topography images of the active layer films at various D1:D2 ratios. The PTB7-Th:COi8DFIC binary film exhibited an average roughness of 5.61 nm. The addition of 20% PBDB-T into the host binary improved the morphology of the ternary blend by showing a reduced surface roughness value of 4.20 nm. A smooth surface was beneficial for facilitating the charge transport from the active layer to the electrodes by minimizing the recombination.[54] Further increase in the PBDB-T content to 80% resulted in an average roughness of 5.13 nm. This could be attributed to the self-aggregation of PBDB-T at room temperature, which was clearly observed from the high roughness value of 5.96 nm in the PBDB-T:COi8DFIC blend.[55] The phase images corresponding to various D1:D2 ratios are presented in Fig. 6 (e–h). Compared to the PTB7-Th:COi8DFIC binary, the ternary blend with 20% PBDB-T exhibited domains suitable for efficient charge transport to the electrodes. As illustrated in Fig. 6(g) and (h), an increase in the PBDB-T content results in the formation of large domains within the active layer blend, which is inadequate for efficient exciton dissociation. The AFM analysis indicated that the inclusion of PTB7-Th in the blend modulated the molecular arrangement of PBDB-T, thereby enhancing the charge transport in the ternary OSC.

To gain more insight into the role of PBDB-T on the exciton generation and charge extraction in ternary OSCs, photocurrent density (J_{ph}) *versus* effective voltage (V_{eff}) analysis was carried out, and the results are presented in Fig. 7(a). Here, J_{ph} is

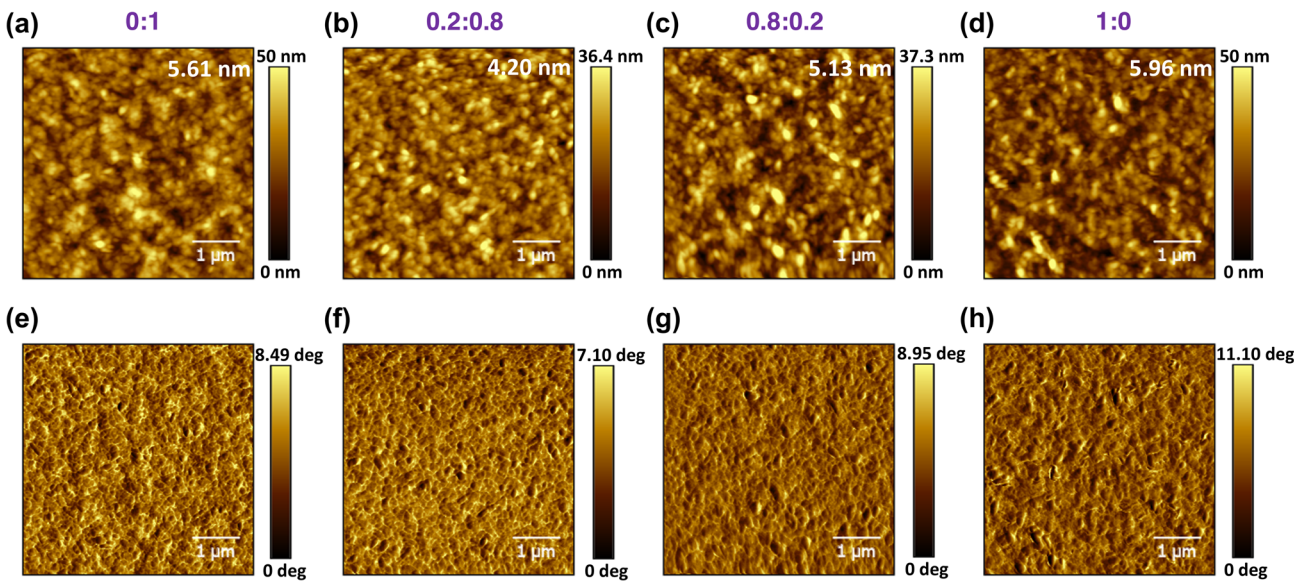

Fig. 6 AFM topography (a–d) and phase (e–h) images of the active layer films corresponding to various PBDB-T:PTB7-Th weight ratios: 0:1, 0.2:0.8, 0.8:0.2, and 1:0.

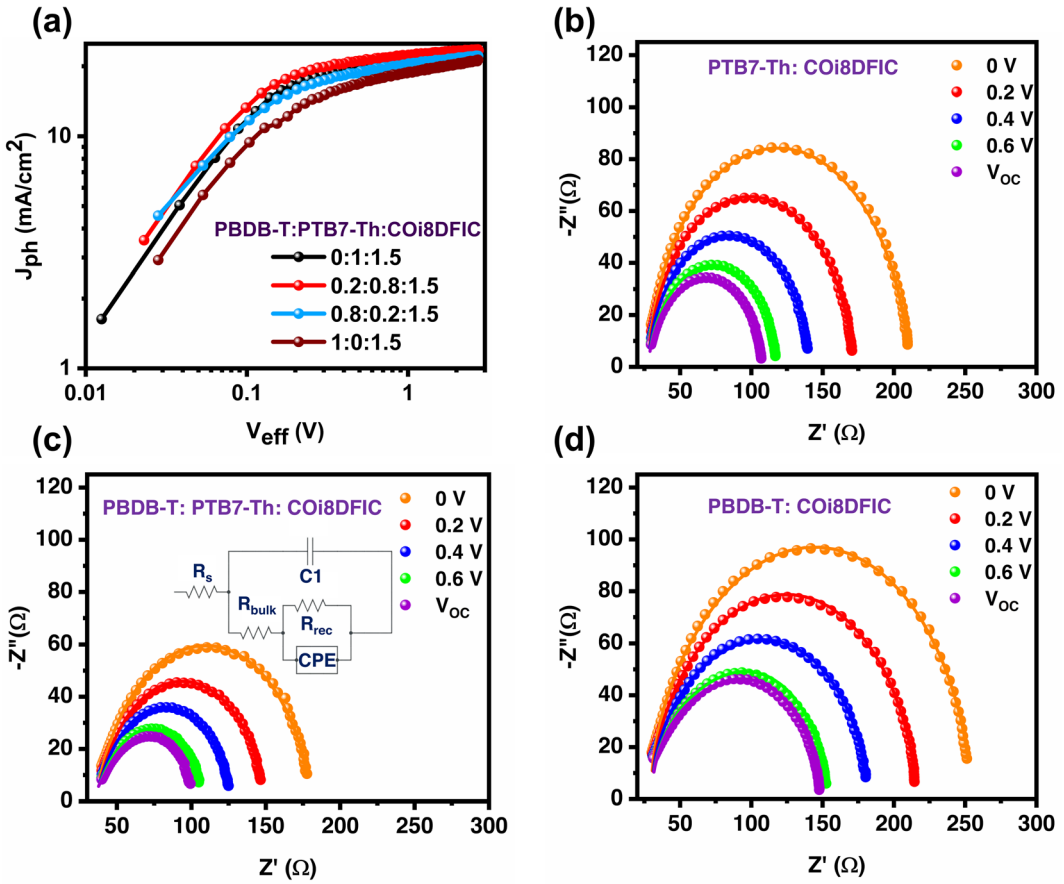

Fig. 7 (a) J_{ph}–V_{eff} curves of OSCs fabricated at various D1:D2 weight ratios. Fitted Nyquist plots of the (b) PTB7-Th:COi8DFIC binary, (c) optimized PBDB-T:PTB7-Th:COi8DFIC ternary and (d) PBDB-T:COi8DFIC binary OSCs.

defined as $J_L - J_D$, where J_L is the current density under 1 sun illumination, and J_D is the current density under dark conditions. V_{eff} is given by $V_0 - V_a$, where V_0 is the voltage at which J_{ph} becomes zero, and V_a is the applied voltage.[56] At $V_{eff} > 2$ V, the high internal field dissociated the excitons into free charge carriers, which were collected at respective electrodes, providing a saturation current density (J_{sat}). Among all the devices, the optimized ternary OSC exhibited the highest J_{sat} value of 23.45 mA cm^{-2} (Table 2) due to enhanced absorption in the active layer blend. The improved FF value observed in the optimized ternary OSC was directly related to the charge transport properties. In order to explore this, exciton dissociation (η_{diss}) and charge collection (η_{cc}) efficiencies were calculated from the $J_{ph} - V_{eff}$ curves and are presented in Table 2. η_{diss} is defined as J_{ph}/J_{sat} under short-circuit conditions, and η_{cc} is defined as J_{ph}/J_{sat} under the maximum power output condition. The PTB7-Th:COi8DFIC-based binary OSC exhibited an η_{diss} value of 90.77%, which improved to 92.92% in the case of optimized ternary OSC with 20% PBDB-T content. The fine D/A phase separation observed from the AFM images substantiated this observation, since the excitons formed in the donor (or acceptor) were dissociated within their exciton dissociation lengths before recombination. As the PBDB-T content increased to 80%, the η_{diss} reduced to 89.85%. Among all the devices, the lowest η_{diss} was observed for the PBDB-T:COi8DFIC-based binary OSC, which was attributed to the inadequate phase separation in the active layer blend, as observed from the AFM analysis. A similar trend was observed in the charge collection, with the optimized ternary exhibiting the highest η_{cc} value of 75.1%, followed by the PTB7-Th:COi8DFIC-based binary (73.5%), ternary OSC containing 80% PBDB-T (72.21%) and PBDB-T:COi8DFIC-based binary (62.9%). These results indicated that the incorporation of a small amount of PBDB-T into the host blend improved the charge transport properties of the ternary OSCs, thereby enhancing the PCE.

The improvement in PCE of the PTB7-Th:COi8DFIC binary OSC upon the addition of PBDB-T was due to the enhancement of J_{SC} and FF, which were directly related to the charge transport and recombination processes in the device. Impedance spectroscopy (IS) analysis is considered a powerful and non-destructive technique to probe various electrical processes in OSCs. In order to get a clear picture of the dynamics of photo-generated charge carriers within the operating regime (0–V_{OC}), the IS measurements were carried out at various bias voltages under 1 sun illumination. The Nyquist plots of the PTB7-Th:COi8DFIC binary, PBDB-T:PTB7-Th:COi8DFIC ternary and PBDB-T:COi8DFIC binary OSCs are presented in Fig. 7 (b–d), respectively. All the Nyquist plots were fitted with the

Table 2 Exciton-dissociation and charge-collection efficiencies calculated from $J_{ph} - V_{eff}$ curves[a,b,c]

PBDB-T:PTB7-Th:COi8DFIC	$J_{ph}^{\#}$(mA cm^{-2})	J_{ph}^{*} (mA cm^{-2})	J_{sat} (mA cm^{-2})	η_{diss} (%)	η_{cc} (%)
0:1:1.5	20.38	16.50	22.45	90.77	73.50
0.2:0.8:1.5	21.79	17.61	23.45	92.92	75.1
0.8:0.2:1.5	19.76	15.88	21.99	89.85	72.21
1:0:1.5	17.84	13.24	21.04	84.5	62.9

[a] $J_{ph}^{\#}$: Photocurrent density at the short circuit condition. [b] J_{ph}^{*}: Photocurrent density at the maximum power point condition. [c] J_{sat}: Photocurrent density at the saturation point.

Matryoshka or ladder-type equivalent circuit, which is shown in the inset of Fig. 7(c).[57,58] The high-frequency region in the Nyquist plot represents charge transport properties, whereas the low-frequency region characterizes various recombination processes present in the device.[59] The bulk (R_{bulk}) and recombination (R_{rec}) resistances, which provide a deeper understanding of charge transport and recombination processes in OSCs, were obtained by fitting the Nyquist plots. The variation of R_{bulk} and R_{rec} with the bias voltage is shown in Fig. 8(a) and (b), respectively. A relatively high R_{bulk} indicates reduced charge transport, whereas a relatively high R_{rec} means low recombination in the device. From Fig. 8(a) and (b), it is clear that the optimum ternary OSC exhibits lower R_{bulk} and higher R_{rec} compared to the two binary devices, indicating efficient charge transport. In order to get a clear picture, the R_{bulk} and R_{rec} of individual devices are compared in Fig. S8. For the PBDB-T:COi8DFIC binary, the R_{bulk} was more than the R_{rec} at all bias voltages, which substantiated the observed low FF values. For both the PTB7-Th:COi8DFIC-based binary and optimum ternary, R_{rec} was found to be higher than R_{bulk}, with the ternary showing a large difference between the two resistances, indicating efficient charge transport. Furthermore, Xu *et al.* reported that the FF in OSC can be directly correlated to $(R_{rec}/R_{bulk})^{1/2}$ value.[60] At 0 V, the PTB7-Th:COi8DFIC-based binary

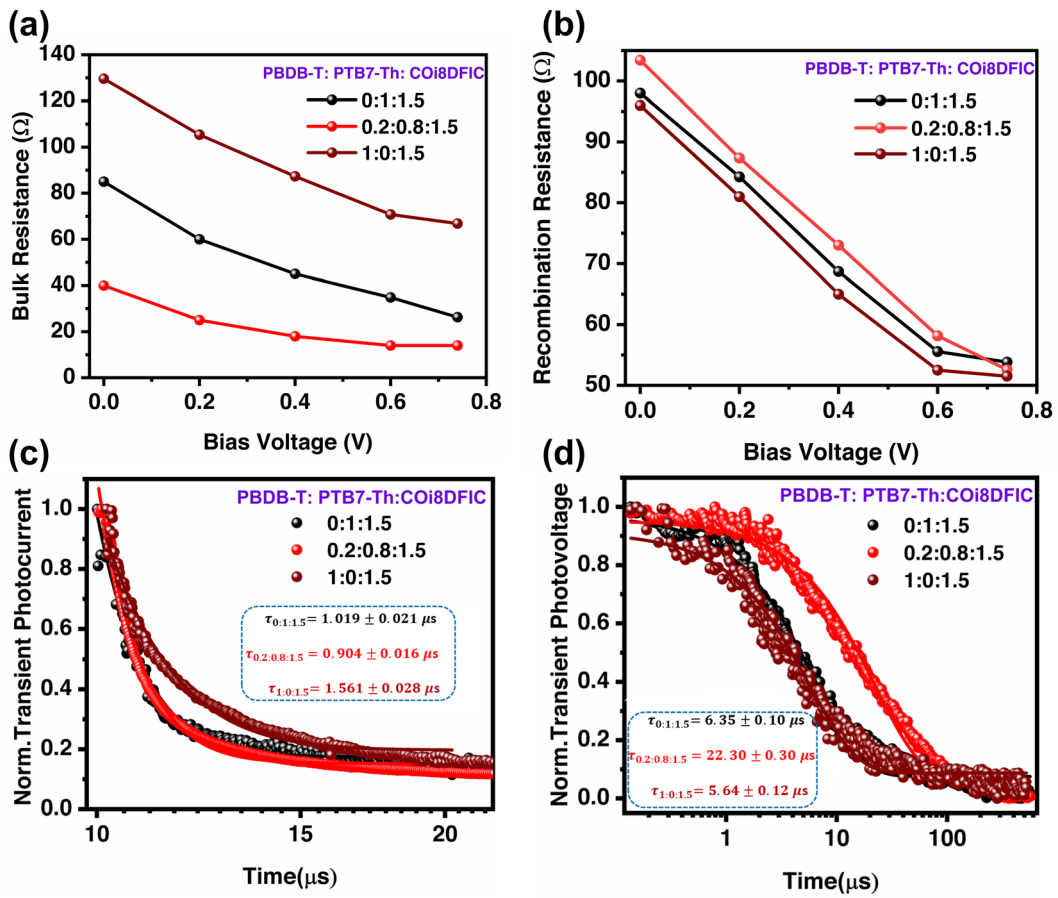

Fig. 8 Variation of the (a) bulk resistance and (b) recombination resistance of OSCs with bias voltage. (c) Transient photocurrent and (d) transient photovoltage curves of binary and ternary OSCs. A constant background light bias with 0.1 sun (~10 mW cm^{-2}) intensity is applied for the measurement.

Table 3 Voltage-loss values for the OSCs with various PBDB-T:PTB7-Th weight ratios

PBDB-T:PTB7-Th:COi8DFIC	E_g (eV)	V_{OC} (V)	$V_{OC,SQ}$ (V)	$V_{OC,rad}$ (V)<	ΔV_1 (V)	ΔV_1 (V)	ΔV_1 (V)
0:1:1.5	1.368	0.721	1.108	1.028	0.260	0.079	0.307
0.2:0.8:1.5	1.366	0.726	1.106	1.029	0.260	0.077	0.303
0.8:0.2:1.5	1.363	0.721	1.103	1.025	0.260	0.079	0.304
1:0:1.5	1.365	0.708	1.105	1.026	0.260	0.078	0.318

exhibited a $(R_{rec}/R_{bulk})^{1/2}$ value of 1.07, which increased to 1.61 for the ternary device, validating the improvement in the FF values for the ternary OSC.

To further understand the consequence of the increased R_{rec} and reduced R_{bulk} observed for the optimal ternary OSC on the charge extraction and charge carrier lifetimes, TPC and TPV measurements were employed.[61] TPC and TPV rely on the measurement of photocurrent and photovoltage response, respectively, to a small light perturbation superimposed on a constant bias light.[62,63] The carrier generation is considered effectively instantaneous.[64,65] However, the perturbation pulse width was chosen so that the device reached steady state before the perturbation was turned off. As a result, the subsequent decay isolates charge extraction (photocurrent) or recombination (photovoltage) processes at various timescales, depending on the external bias of the device.[66–68] During TPC measurement, the device was held under short-circuit conditions, and the resulting decay profile provided information about the charge extraction lifetime. In the TPV measurements, the device was kept under open-circuit conditions to determine the charge-carrier lifetimes.[69,70] The TPC and TPV decay profiles of the PTB7-Th:COi8DFIC, PBDB-T:COi8DFIC binary and PBDBT:PTB7-Th:COi8DFIC (0.2:0.8:1.5) ternary devices are presented in Fig. 8(c) and (d), respectively. The TPC decay profiles for a background light with 0.1 sun intensity were used to extract the charge carrier lifetimes (see the SI). The results revealed that the ternary system had a faster carrier extraction time of $\tau_{ternary} = 904 \pm 16$ ns than the control binary ($\tau_{PTB7\text{-}Th,\ binary} = 1019 \pm 21$ ns). On the other hand, the PBDB-T:COi8DFIC-based binary device exhibited a relatively poor extraction time of 1561 ± 28 ns. The quick carrier extraction observed in the optimal ternary device indicated reduced charge carrier resistance, substantiating the observed improvement in the FF and the J_{SC}.[71] From the TPV curves displayed in Fig. 8(d), the charge carrier lifetime of the PTB7-Th:COi8DFIC-based host binary was found to increase from 6.35 ± 0.10 μs to 22.30 ± 0.30 μs upon the addition of 20 wt% PBDB-T. However, the PBDB-T:COi8DFIC-based binary showed the lowest charge carrier lifetime ($\tau_{PBDB\text{-}T,\ binary} = 5.64 \pm 0.12$ μs), thereby validating the high bulk and low recombination resistances obtained from impedance analysis. The improved charge carrier lifetime observed for the optimum ternary device indicated reduced recombination losses. Hence the increase in the charge carrier lifetime, along with a short extraction time, helped the ternary OSC to reduce its recombination losses to enhance FF and $J_{SC,}$ thereby improving the PCE.

In order to understand the causal relationship between recombination, charge transport and the proposed energy transfer mechanism, a qualitative voltage-loss analysis was performed. The total voltage loss in a solar cell is represented as $\Delta V = \Delta V_1 + \Delta V_2 + \Delta V_3$, where $\Delta V_1 = \frac{E_g}{q} - V_{oc,\ SQ}$, which is the radiative loss above the optical bandgap, and it is the fundamental loss in all solar cells. Here, E_g is the optical bandgap, q is the elementary charge and $V_{oc,\ SQ}$ is the maximum open-circuit voltage that a solar cell can achieve, as predicted by Shockley and Queisser. $\Delta V_2 = V_{oc,\ SQ} - V_{oc,\ rad}$ represents the radiative recombination below the optical bandgap. ΔV_3 quantifies the non-radiative recombination loss in a solar cell, and it is defined as $\Delta V_3 = V_{oc,rad} - V_{oc}$.[72] As shown in Table 3, ΔV_1 (~0.26 V) and ΔV_2 (~0.08 V) remain nearly unchanged for all devices, indicating that the optical gap and radiative recombination processes are not significantly influenced by the addition of PBDB-T. In contrast, a considerable change in ΔV_3 was observed across the devices. Compared to the PTB7-Th:COi8DFIC-based host binary with a ΔV_3 value of 0.307 V, the optimum ternary exhibited a relatively low ΔV_3 value of 0.303 V. The reduced ΔV_3 provided direct quantitative evidence that FRET suppresses non-radiative recombination by facilitating rapid exciton energy transfer prior to thermal relaxation and trap-assisted decay. This reduction in the non-radiative recombination is consistent with the decreased bulk resistance and prolonged carrier lifetime observed in impedance spectroscopy and transient measurements. The present study reports the utilization of a wide bandgap polymer donor for the efficiency enhancement of the PTB7-Th:COi8DFIC-based OSCs. In addition to high efficiency, long-term stability and scalability play a crucial role in the commercialization of OSCs. The variation of the efficiency with the active-layer thickness and the device area and the effect of illumination and thermal exposure on the long-term stability need to be thoroughly investigated.

4. Conclusions

In summary, the PCE of the PTB7-Th:COi8DFIC-based binary OSC was successfully improved by incorporating a wide-bandgap donor, PBDB-T, as the third component. The addition of 20 wt% PBDB-T into the host blend resulted in an average PCE of 9.74%, owing to the improvement of J_{SC} and FF. The PCE enhancement was primarily attributed to the efficient utilization of high-energy photons through an energy-transfer mechanism, as confirmed by steady-state and time-resolved photoluminescence measurements. AFM analysis revealed the formation of an optimized active layer morphology upon the introduction of a small amount of PBDB-T, which noticeably improved the exciton-dissociation and charge-collection efficiencies in the ternary OSC. The observed enhancement of J_{SC} and FF was validated by low bulk and high recombination

resistances obtained from impedance spectroscopy measurements. Importantly, a fast charge extraction (≈904 ns) and enhanced carrier lifetime (≈22.30 μs) were achieved with the optimized ternary devices, consistent with the enhanced device performance. Voltage-loss analysis revealed a slight suppression of the non-radiative recombination in the optimum ternary device compared to the host binary. The present study shows that the ternary strategy is an effective method for improving the performance of the PTB7-Th:COi8DFIC-based OSC, combining superior energy transfer with optimized morphology and broadband absorption.

Author contributions

Anoop C Sathyadevan Nair: data curation (lead); formal analysis (lead); investigation (lead); writing – original draft (lead). K P Adarsh Raj: data curation (supporting); formal analysis (supporting); investigation (supporting). Muneendra Dasannagari: data curation (supporting); formal analysis (supporting); writing – original draft (supporting). Abhijith T: formal analysis (supporting); writing – review & editing (equal). Abhishek Melarkode Rajendran: investigation (supporting). Dipangkor Basumatary: formal analysis (supporting). Safakath Karuthedath: supervision (supporting); writing – review & editing (equal). C. S. Suchand Sangeeth: conceptualization (supporting); supervision (supporting); writing – review & editing (equal). Vari Sivaji Reddy: funding acquisition (lead); project administration (lead); conceptualization (lead); supervision (lead); writing – review & editing (equal). All authors have given approval to the final version of the manuscript.

Conflicts of interest

There are no conflicts to declare.

Data availability

The data supporting this article have been included as part of the supplementary information (SI). Supplementary information is available. See DOI: https://doi.org/10.1039/d5ra08837b.

Acknowledgements

The authors thank the Science and Engineering Research Board (SERB), India, for supporting this work under the Core Research Grant (CRG) (Project File No. CRG/2021/001795). The EQE facility at CeNSE, IISc Bangalore, the steady-state PL measurement facility at SAIF, M G University, Kottayam, and the AFM facility at PSGIAS are gratefully acknowledged. The authors acknowledge Mr Shyam Sankar S and Prof. G.D. Sharma (LNMIIT, Rajasthan) for TRPL measurements, Dr Subramanyan N. V. for contact angle measurements and Dr Rakesh Suthar for voltage-loss analysis.

References

1 F. Zhao, J. Zhou, D. He, C. Wang and Y. Lin, Low-Cost Materials for Organic Solar Cells, *J. Mater. Chem. C*, 2021, **9**(43), 15395–15406.
2 N. Yang, S. Zhang, Y. Cui, J. Wang, S. Cheng and J. Hou, Molecular Design for Low-Cost Organic Photovoltaic Materials, *Nat. Rev. Mater.*, 2025, **10**(6), 404–424.
3 F. Yang, Y. Huang, Y. Li and Y. Li, Large-Area Flexible Organic Solar Cells, *npj Flex. Electron.*, 2021, **5**(1), 30.
4 L. Sun, K. Fukuda and T. Someya, Recent Progress in Solution-Processed Flexible Organic Photovoltaics, *npj Flex. Electron.*, 2022, **6**(1), 89.
5 B. Zhang, F. Yang and Y. Li, Recent Progress in Large-Area Organic Solar Cells, *Small Sci.*, 2023, **3**(7), 2300004.
6 M. S. Vezie, S. Few, I. Meager, G. Pieridou, B. Dörling, R. S. Ashraf, A. R. Goñi, H. Bronstein, I. McCulloch, S. C. Hayes, M. Campoy-Quiles and J. Nelson, Exploring the Origin of High Optical Absorption in Conjugated Polymers, *Nat. Mater.*, 2016, **15**(7), 746–753.
7 H. Zhang, S. Jia, Z. Liu and Z. Chen, Ternary Organic Solar Cells by Small Amount of Efficient Light Absorption Polymer PSEHTT as Third Component Materials, *Molecules*, 2023, **28**(19), 6832.
8 G. Zhang, J. Zhao, P. C. Y. Chow, K. Jiang, J. Zhang, Z. Zhu, J. Zhang, F. Huang and H. Yan, Nonfullerene Acceptor Molecules for Bulk Heterojunction Organic Solar Cells, *Chem. Rev.*, 2018, **118**(7), 3447–3507.
9 J. Hou, O. Inganäs, R. H. Friend and F. Gao, Organic Solar Cells Based on Non-Fullerene Acceptors, *Nat. Mater.*, 2018, **17**(2), 119–128.
10 Y. Zhang, Y. Wang, T. Shan, Q. Wei, Y. X. Xu and H. Zhong, Non-Fullerene Acceptors with an Optical Response over 1000 Nm toward Efficient Organic Solar Cells, *ACS Appl. Mater. Interfaces*, 2021, **13**(43), 51279–51288.
11 M. W. Wanlass, K. A. Emery, T. A. Gessert, G. S. Horner, C. R. Osterwald and T. J. Coutts, Practical Considerations in Tandem Cell Modeling, *Sol. Cell.*, 1989, **27**(1–4), 191–204.
12 A. Yakimov and S. R. Forrest, High Photovoltage Multiple-Heterojunction Organic Solar Cells Incorporating Interfacial Metallic Nanoclusters, *Appl. Phys. Lett.*, 2002, **80**(9), 1667–1669.
13 J. Y. Kim, K. Lee, N. E. Coates, D. Moses, T.-Q. Nguyen, M. Dante and A. J. Heeger, Efficient Tandem Polymer Solar Cells Fabricated by All-Solution Processing, *Science*, 2007, **317**(5835), 222–225.
14 M. K. Siddiki, J. Li, D. Galipeau and Q. Qiao, A Review of Polymer Multijunction Solar Cells, *Energy Environ. Sci.*, 2010, **3**(7), 867.
15 T. Ameri, G. Dennler, C. Lungenschmied and C. J. Brabec, Organic Tandem Solar Cells: A Review, *Energy Environ. Sci.*, 2009, **2**(4), 347.
16 P. Suresh, P. Balraju, G. D. Sharma, J. A. Mikroyannidis and M. M. Stylianakis, Effect of the Incorporation of a Low-Band-Gap Small Molecule in a Conjugated Vinylene Copolymer:

PCBM Blend for Organic Photovoltaic Devices, *ACS Appl. Mater. Interfaces*, 2009, **1**(7), 1370–1374.
17 N. Gasparini, A. Salleo, I. McCulloch and D. Baran, The Role of the Third Component in Ternary Organic Solar Cells, *Nat. Rev. Mater.*, 2019, **4**(4), 229–242.
18 C. Zhao, J. Wang, X. Zhao, Z. Du, R. Yang and J. Tang, Recent Advances, Challenges and Prospects in Ternary Organic Solar Cells, *Nanoscale*, 2021, **13**(4), 2181–2208.
19 N. Sun, L. Tang, L. Yang, M. Du, Z. Wang, Q. Guo, P. Cong, Y. Geng, J. Du and E. Zhou, Ternary Organic Solar Cells Containing Fused-Benzotriazole Polymer as Donor and Two Types of Benzotriazole Molecules as Guest Component, *Chem. Eng. J.*, 2025, **503**, 158661.
20 N. Y. Doumon, L. Yang and F. Rosei, Ternary Organic Solar Cells: A Review of the Role of the Third Element, *Nano Energy*, 2022, **94**, 106915.
21 R. Yu, H. Yao and J. Hou, Recent Progress in Ternary Organic Solar Cells Based on Nonfullerene Acceptors, *Adv. Energy Mater.*, 2018, **8**(28), 1702814.
22 M. Günther, N. Kazerouni, D. Blätte, J. D. Perea, B. C. Thompson and T. Ameri, Models and Mechanisms of Ternary Organic Solar Cells, *Nat. Rev. Mater.*, 2023, **8**(7), 456–471.
23 D. Zhou, W. You, H. Xu, Y. Tong, B. Hu, Y. Xie and L. Chen, Recent Progress in Ternary Organic Solar Cells Based on Solution-Processed Non-Fullerene Acceptors, *J. Mater. Chem. A*, 2020, **8**(44), 23096–23122.
24 J. Zhou, X. Zhou, H. Jia, L. Tu, S. Wu, X. Xia, X. Song and Y. Shi, 20.0% Efficiency of Ternary Organic Solar Cells Enabled by a Novel Wide Band Gap Polymer Guest Donor, *Energy Environ. Sci.*, 2025, **18**(7), 3341–3351.
25 H. Chen, Y. Huang, R. Zhang, H. Mou, J. Ding, J. Zhou, Z. Wang, H. Li, W. Chen, J. Zhu, Q. Cheng, H. Gu, X. Wu, T. Zhang, Y. Wang, H. Zhu, Z. Xie, F. Gao, Y. Li and Y. Li, Organic Solar Cells with 20.82% Efficiency and High Tolerance of Active Layer Thickness through Crystallization Sequence Manipulation, *Nat. Mater.*, 2025, **24**(3), 444–453.
26 H. Xia, C. You, J. Fu, D. Luo, R. Ma, H. Liu, Y. Lang, X. Lu, W. Zhu and G. Li, Unveiling Energy Loss Mechanisms to Empower Ternary Organic Solar Cells with over 20% Efficiency: A Systematic Oligomeric Approach, *Adv. Mater.*, 2025, 2501428.
27 Y. Jiang, S. Sun, R. Xu, F. Liu, X. Miao, G. Ran, K. Liu, Y. Yi, W. Zhang and X. Zhu, Non-fullerene acceptor with asymmetric structure and phenyl-substituted alkyl side chain for 20.2% efficiency organic solar cells, *Nat. Energy*, 2024, **9**(8), 975–986.
28 Z. Xiao, X. Jia, D. Li, S. Wang, X. Geng, F. Liu, J. Chen, S. Yang, T. P. Russell and L. Ding, 26 mA Cm−2 Jsc from Organic Solar Cells with a Low-Bandgap Nonfullerene Acceptor, *Sci. Bull.*, 2017, **62**(22), 1494–1496.
29 D. Khlaifia and K. Alimi, PTB7-Th/Non-Fullerene Acceptors for Organic Solar Cells, *Synth. Met.*, 2022, **291**, 117189.
30 W. Li, M. Chen, J. Cai, E. L. K. Spooner, H. Zhang, R. S. Gurney, D. Liu, Z. Xiao, D. G. Lidzey, L. Ding and T. Wang, Molecular Order Control of Non-Fullerene Acceptors for High-Efficiency Polymer Solar Cells, *Joule*, 2019, **3**(3), 819–833.
31 X. Zhang, H. Wang, D. Li, M. Chen, Y. Mao, B. Du, Y. Zhuang, W. Tan, W. Huang, Y. Zhao, D. Liu and T. Wang, Modulation of J-Aggregation of Nonfullerene Acceptors toward Near-Infrared Absorption and Enhanced Efficiency, *Macromolecules*, 2020, **53**(10), 3747–3755.
32 S. Karuthedath, S. H. K. Paleti, A. Sharma, H. Yin, C. S. P. De Castro, S. Chen, H. Xu, N. Alshehri, N. Ramos, J. I. Khan, J. Martin, G. Li, F. Laquai, D. Baran and J. Gorenflot, Rationalizing the Influence of Tunable Energy Levels on Quantum Efficiency to Design Optimal Non-Fullerene Acceptor-Based Ternary Organic Solar Cells, *Adv. Energy Mater.*, 2023, **13**(16), 2203464.
33 Y. Huang, A. Azeez, J. Zhao, Z. Zhao, M. Dasannagari, F. Laquai, Z. Kan and S. Karuthedath, Enhanced Device Performance through Optimization of Acceptor Layer Thickness Relative to Exciton Diffusion Length and Ionization Energy Offset in Bilayer Organic Solar Cells, *J. Mater. Chem. C*, 2025, **13**(11), 5911–5919.
34 X. Ma, Z. Xiao, Q. An, M. Zhang, Z. Hu, J. Wang, L. Ding and F. Zhang, Simultaneously Improved Efficiency and Average Visible Transmittance of Semitransparent Polymer Solar Cells with Two Ultra-Narrow Bandgap Nonfullerene Acceptors, *J. Mater. Chem. A*, 2018, **6**(43), 21485–21492.
35 C. Yang, Y. Sun, Q. Li, K. Liu, X. Xue, Y. Huang, K. Ren, L. Li, Y. Chen, Z. Wang, S. Qu and Z. Wang, Nonfullerene Ternary Organic Solar Cell with Effective Charge Transfer between Two Acceptors, *J. Phys. Chem. Lett.*, 2020, **11**(3), 927–934.
36 Z. Xiao, X. Jia and L. Ding, Ternary Organic Solar Cells Offer 14% Power Conversion Efficiency, *Sci. Bull.*, 2017, **62**(23), 1562–1564.
37 L. Duan, X. Meng, Y. Zhang, H. Yi, K. Jin, F. Haque, C. Xu, Z. Xiao, L. Ding and A. Uddin, Comparative Analysis of Burn-in Photo-Degradation in Non-Fullerene COi8DFIC Acceptor Based High-Efficiency Ternary Organic Solar Cells, *Mater. Chem. Front.*, 2019, **3**(6), 1085–1096.
38 C. M. Nkinyam, C. O. Ujah, K. C. Nnakwo and D. V. V. Kallon, Insight into Organic Photovoltaic Cell: Prospect and Challenges, *Unconv. Resour.*, 2025, **5**, 100121.
39 V. Papamakarios, E. Polydorou, A. Soultati, N. Droseros, D. Tsikritzis, A. M. Douvas, L. Palilis, M. Fakis, S. Kennou, P. Argitis and M. Vasilopoulou, Surface Modification of ZnO Layers via Hydrogen Plasma Treatment for Efficient Inverted Polymer Solar Cells, *ACS Appl. Mater. Interfaces*, 2016, **8**(2), 1194–1205.
40 V. Gupta, V. Bharti, M. Kumar, S. Chand and A. J. Heeger, Polymer–Polymer Förster Resonance Energy Transfer Significantly Boosts the Power Conversion Efficiency of Bulk-Heterojunction Solar Cells, *Adv. Mater.*, 2015, **27**(30), 4398–4404.
41 Z. Li, X. Xu, W. Zhang, X. Meng, Z. Genene, W. Ma, W. Mammo, A. Yartsev, M. R. Andersson, R. A. J. Janssen and E. Wang, 9.0% Power Conversion Efficiency from Ternary All-Polymer Solar Cells, *Energy Environ. Sci.*, 2017, **10**(10), 2212–2221.

42 H. Wang, D. Yang, P. Ding, L. Xie, Z. Chen, S. Yang, P. Yan, Y. Meng, J. Zhang, Z. Wei and Z. Ge, Dual Förster Resonance Energy Transfer Effects Enables High Photocurrent Density and High Fill Factor in Ternary Organic Solar Cells, *Chem. Eng. J.*, 2023, **474**, 145395.
43 W. Xu, T. Du, M. Sachs, T. J. Macdonald, G. Min, L. Mohan, K. Stewart, C.-T. Lin, J. Wu, R. Pacalaj, S. A. Haque, M. A. McLachlan and J. R. Durrant, Asymmetric Charge Carrier Transfer and Transport in Planar Lead Halide Perovskite Solar Cells, *Cell Rep. Phys. Sci.*, 2022, **3**(5), 100890.
44 L. Guguloth, K. Singh, V. S. R. Channu and K. Kumari, Enhancement in Performance of Ternary Blend-Polymer Solar Cells Using a PEDOT:PSS–Graphene Oxide Hole Transport Layer *via* Förster Resonance Energy Transfer and Balanced Charge Transport, *Mater. Adv.*, 2020, **1**(8), 2872–2887.
45 Y. Xie, T. Li, J. Guo, P. Bi, X. Xue, H. S. Ryu, Y. Cai, J. Min, L. Huo, X. Hao, H. Y. Woo, X. Zhan and Y. Sun, Ternary Organic Solar Cells with Small Nonradiative Recombination Loss, *ACS Energy Lett.*, 2019, **4**(5), 1196–1203.
46 L. Xiao, X. Wu, G. Ren, M. A. Kolaczkowski, G. Huang, W. Tan, L. Ma, Y. Liu, X. Peng, Y. Min and Y. Liu, Highly Efficient Ternary Solar Cells with Efficient Förster Resonance Energy Transfer for Simultaneously Enhanced Photovoltaic Parameters, *Adv. Funct. Mater.*, 2021, **31**(41), 2105304.
47 M. Zhou, K. Zhang, X. Li, Y. Ge, W. Zhang, P. Lu and X. Hao, Improved Exciton Diffusion through Modulating Förster Resonance Energy Transfer for Efficient Organic Solar Cells, *Sol. RRL*, 2024, **8**(13), 2400136.
48 Q. An, F. Zhang, L. Li, J. Wang, J. Zhang, L. Zhou and W. Tang, Improved Efficiency of Bulk Heterojunction Polymer Solar Cells by Doping Low-Bandgap Small Molecules, *ACS Appl. Mater. Interfaces*, 2014, **6**(9), 6537–6544.
49 A. Kozbial, Z. Li, C. Conaway, R. McGinley, S. Dhingra, V. Vahdat, F. Zhou, B. D'Urso, H. Liu and L. Li, Study on the Surface Energy of Graphene by Contact Angle Measurements, *Langmuir*, 2014, **30**(28), 8598–8606.
50 M. Annamalai, K. Gopinadhan, S. A. Han, S. Saha, H. J. Park, E. B. Cho, B. Kumar, A. Patra, S.-W. Kim and T. Venkatesan, Surface Energy and Wettability of van Der Waals Structures, *Nanoscale*, 2016, **8**(10), 5764–5770, DOI: 10.1039/C5NR06705G.
51 S. Wu, Calculation of Interfacial Tension in Polymer Systems, *J. Polym. Sci., C Polym. Symp.*, 1971, **34**(1), 19–30.
52 A. C. Sathyadevan Nair, P. . , A. R. K, A. Thazhathenair, S. Shankar S, A. M. Rajendran, D. Basumatary, G. D. Sharma, C. S. Suchand Sangeeth and V. S. Reddy, Energy Transfer and Donor Alloy Synergy for Performance Enhancement of Ternary Organic Solar Cells, *ACS Appl. Polym. Mater.*, 2025, **7**(24), 16939–16947.
53 P. Bi, S. Zhang, Z. Chen, Y. Xu, Y. Cui, T. Zhang, J. Ren, J. Qin, L. Hong, X. Hao and J. Hou, Reduced Non-Radiative Charge Recombination Enables Organic Photovoltaic Cell Approaching 19% Efficiency, *Joule*, 2021, **5**(9), 2408–2419.
54 Y. Zhang, X. Li, T. Dai, D. Xu, J. Xi and X. Chen, Charge Transport and Extraction of PTB7:PC_{71} BM Organic Solar Cells: Effect of Film Thickness and Thermal-Annealing, *RSC Adv.*, 2019, **9**(43), 24895–24903.
55 B. Du, R. Geng, W. Tan, Y. Mao, D. Li, X. Zhang, D. Liu, W. Tang, W. Huang and T. Wang, Heating Induced Aggregation in Non-Fullerene Organic Solar Cells towards High Performance, *J. Energy Chem.*, 2021, **54**, 131–137.
56 F. G. Guijarro, P. De La Cruz, K. Khandelwal, R. Singhal, F. Langa and G. D. Sharma, Effects of Halogenation on Cyclopentadithiophenevinylene-Based Acceptors with Excellent Responses in Binary Organic Solar Cells, *ACS Appl. Mater. Interfaces*, 2023, **15**(17), 21296–21305.
57 A. Todinova, L. Contreras-Bernal, M. Salado, S. Ahmad, N. Morillo, J. Idígoras and J. A. Anta, Towards a Universal Approach for the Analysis of Impedance Spectra of Perovskite Solar Cells: Equivalent Circuits and Empirical Analysis, *Chemelectrochem*, 2017, **4**(11), 2891–2901.
58 Y. Alishan, A. Joseph, A. B. Pillai, R. K. Aparna, R. Sarkar, S. Chakraborty, S. Mandal and M. A. G. Namboothiry, Metal Nanoclusters for Interface Engineering and Improved Photovoltaic Performance in Organic Solar Cells, *ACS Nano*, 2024, **18**(52), 35383–35392.
59 B. Anitha, K. P. Vijith, A. Alexander, V. Srivastava and M. A. G. Namboothiry, Understanding the Poor Fill Factor of Solution-Processed Squaraine Based Solar Cells in Terms of Charge Carrier Dynamics Probed *via* Impedance and Transient Spectroscopy, *J. Mater. Chem. C*, 2020, **8**(42), 14748–14756.
60 L. Xu, Y.-J. Lee and J. W. P. Hsu, Charge Collection in Bulk Heterojunction Organic Photovoltaic Devices: An Impedance Spectroscopy Study, *Appl. Phys. Lett.*, 2014, **105**(12), 123904.
61 J. Bisquert and M. Janssen, From Frequency Domain to Time Transient Methods for Halide Perovskite Solar Cells: The Connections of IMPS, IMVS, TPC, and TPV, *J. Phys. Chem. Lett.*, 2021, **12**(33), 7964–7971.
62 B. C. O'Regan and F. Lenzmann, Charge Transport and Recombination in a Nanoscale Interpenetrating Network of N-Type and p-Type Semiconductors: Transient Photocurrent and Photovoltage Studies of TiO_2/Dye/CuSCN Photovoltaic Cells, *J. Phys. Chem. B*, 2004, **108**(14), 4342–4350.
63 M. Azzouzi, P. Calado, A. M. Telford, F. Eisner, X. Hou, T. Kirchartz, P. R. F. Barnes and J. Nelson, Overcoming the Limitations of Transient Photovoltage Measurements for Studying Recombination in Organic Solar Cells, *Sol. RRL*, 2020, **4**(5), 1900581.
64 M. Pranav, A. Shukla, D. Moser, J. Rumeney, W. Liu, R. Wang, B. Sun, S. Smeets, N. Tokmoldin, Y. Cao, G. He, T. Beitz, F. Jaiser, T. Hultzsch, S. Shoaee, W. Maes, L. Lüer, C. Brabec, K. Vandewal, D. Andrienko, S. Ludwigs and D. Neher, On the Critical Competition between Singlet Exciton Decay and Free Charge Generation in Non-Fullerene Based Organic Solar Cells with Low Energetic Offsets, *Energy Environ. Sci.*, 2024, **17**(18), 6676–6697.
65 C. Deibel and V. Dyakonov, Polymer–Fullerene Bulk Heterojunction Solar Cells, *Rep. Prog. Phys.*, 2010, **73**(9), 096401.

66 Z. Zhao, S. Chung, L. Bai, J. Zhang, Y. Liu, L. Tan, A. Azeez, Y. Huang, E. Ok, K. Cho, Z. Kan and S. Karuthedath, Solubility-Driven Acceptor Fibrilization Enables Bilayer Organic Solar Cells with Efficiency Approaching 20%, *Adv. Funct. Mater.*, 2025, 2506593.

67 J. Wu, H. Cha, T. Du, Y. Dong, W. Xu, C. Lin and J. R. Durrant, A Comparison of Charge Carrier Dynamics in Organic and Perovskite Solar Cells, *Adv. Mater.*, 2022, **34**(2), 2101833.

68 J. Vollbrecht, N. Tokmoldin, B. Sun, V. V. Brus, S. Shoaee and D. Neher, Determination of the Charge Carrier Density in Organic Solar Cells: A Tutorial, *J. Appl. Phys.*, 2022, **131**(22), 221101.

69 T. Zhu, L. Zheng, Z. Xiao, X. Meng, L. Liu, L. Ding and X. Gong, Functionality of Non-Fullerene Electron Acceptors in Ternary Organic Solar Cells, *Sol. RRL*, 2019, **3**(12), 1900322.

70 E. Palomares, N. F. Montcada, M. Méndez, J. Jiménez-López, W. Yang, G. Boschloo, Photovoltage/Photocurrent Transient Techniques, In *Characterization Techniques for Perovskite Solar Cell Materials*, Elsevier, 2020, pp. 161–180.

71 Y. Firdaus, V. M. Le Corre, J. I. Khan, Z. Kan, F. Laquai, P. M. Beaujuge and T. D. Anthopoulos, Key Parameters Requirements for Non-Fullerene-Based Organic Solar Cells with Power Conversion Efficiency >20%, *Adv. Sci.*, 2019, **6**(9), 1802028.

72 Y. Cui, Z. Chai, S. Zhu, Z. Wu, H. Xie and H. Hu, Non-Radiative Recombination Energy Losses in Y-Series Asymmetric Acceptor-Based Organic Solar Cells, *Mater. Horiz.*, 2026, **13**(1), 177–193.